Electronic Supplementary Material (ESI) for Organic Chemistry Frontiers.

Supporting Information

Lamellar assembly and nanostructures of amphiphilic boron(III) diketonates through suitable non-covalent interactions

Jingjie Cao,[ab] Chun-Ting Poon,[b] Michael Ho-Yeung Chan,[b] Eugene Yau-Hin Hong,[b] Yat-Hin Cheng,[b] Franky Ka-Wah Hau,[b] Lixin Wu*[a] and Vivian Wing-Wah Yam*[ab]

[a]State Key Laboratory of Supramolecular Structure and Materials and College of Chemistry, Jilin University, Changchun 130012, P. R. China.

[b]Institute of Molecular Functional Materials and Department of Chemistry, The University of Hong Kong, Pokfulam Road, Hong Kong, P. R. China.

Contents

S1. Photophysical Measurements and Instrumentation

^{1}H and $^{13}C\{^{1}H\}$ NMR spectra were recorded on a Bruker AVANCE 400 (400 MHz), or a Bruker DRX 500 (500 MHz) Fourier-transform NMR spectrometer with chemical shifts (δ, ppm) relative to tetramethylsilane (Me_4Si). 1D nuclear Overhauser effect (NOE) experiments were recorded on the 600 MHz FT NMR spectrometer. Positive-ion fast atom bombardment (FAB) mass spectra were recorded on a Thermo Scientific DFS High-Resolution Magnetic Sector mass spectrometer while positive-ion electrospray ionization (ESI) mass spectra were recorded on a Bruker maXis II high-resolution ESI-QTOF mass spectrometer. The UV−visible absorption spectra were recorded on a Varian Cary 50 or a Varian Cary 60 UV−vis spectrophotometer. The temperature-dependent UV−vis absorption spectra were obtained using a Varian Cary 50 UV−vis spectrophotometer equipped with a Varian Cary single cell peltier thermostat. Steady-state excitation and emission spectra at room temperature were obtained on an Edinburgh Instruments FS5 spectrofluorometer. Relative luminescence quantum yields were measured by the optical dilute method reported by Demas and Crosby.[1] An aqueous solution of quinine sulfate in 0.5 M sulfuric acid (excitation wavelength = 365 nm, $\phi = 0.546$) was used as the reference and corrected for the refractive index of the solution.[2] Dynamic light scattering (DLS) measurements were performed by using a Malvern Zetasizer NanoZS instrument. FT-IR spectra (CaF_2 pellet) were collected on a Bruker Vertex 80 V spectrometer (Germany) equipped with DTGS detector (32 scans) in a resolution of 4 cm^{-1}. TEM images were obtained with a JEM-2100F electron microscope operating at 200 kV. Atomic force microscope (AFM) measurements were carried out on a Bruker FastScan atomic force microscope. Powder X-ray diffraction (XRD) data were recorded on a Rigaku X-ray diffractometer using Cu-Kα radiation at a wavelength of 1.542 Å.

S2. Temperature-Dependent Nucleation–Elongation Model and Isodesmic Model in Curve Fitting

Temperature-dependent nucleation-elongation model[3] or isodesmic model[4] both developed by Meijer and coworkers have been applied to fit the experimental data in the variable–temperature UV−vis spectroscopic studies for all the compounds in THF−water mixtures. All cooling curves are obtained at a slow cooling rate of 0.25 K min^{-1} to ensure the self-assembly processes were under thermodynamic control.[1]

A. Nucleation-Elongation Model

The nucleation and elongation regimes are governed by the following equations (1) and (2) respectively.

$$\phi_n = K_a^{1/3}\, exp[(2/3\, K_a^{-1/3} - 1)\frac{h_e}{RT_e^2}\,(T - T_e)] \quad (1)$$

$$\phi_n = \phi_{SAT}\,(1 - exp[-\frac{h_e}{RT_e^2}(T - T_e)]) \quad (2)$$

ϕ_n is the degree of aggregation, and ϕ_{SAT} is a factor introduced to the equation such that ϕ_n/ϕ_{SAT} does not exceed unity. h_e is the molecular enthalpy released due to non-covalent interactions during the elongation process, T_e is the elongation temperature, K_a is the dimensionless equilibrium constant of the nucleation process at T_e and R is the universal gas constant.

Moreover, the number-averaged degree of polymerization averaged over all active species in the elongation regime at a temperature T, $<N_n>$, is given by equation (3) below:

$$<N_n(T)> = \frac{1}{\sqrt{K_a}}\frac{\phi_n}{\phi_{SAT} - \phi_n} \quad (3)$$

whereas the number-averaged degree of polymerization is averaged over all active nucleated species at T_e, and is given by equation (4) as follows:

$$<N_n(T)> = \frac{1}{\sqrt[3]{K_a}} \quad (4)$$

B. Isodesmic Model

The self-assembly process undergoes isodesmic growth mechanism if every monomer addition to the supramolecular polymer is governed by a single equilibrium constant K_e. It is also known as the equal-K model.[4]

In an isodesmic mechanism, the degree of aggregation, α, is related to temperature T by equation (5) below:

$$\alpha(T) = \frac{1}{1 + exp[-0.908\Delta H\frac{T - T_m}{RT_m^2}]} \quad (5)$$

T_m is the melting temperature defined as the temperature when $\alpha = 0.5$, while the molar enthalpy release (ΔH) is related to the formation of non-covalent interactions during the aggregation process. R is the universal gas constant.

The above equation could be utilized to fit the experimental data obtained from the UV-vis absorption change at different temperature such that ΔH and T_m could be obtained.

Furthermore, the average stack length DP_N as well as the equilibrium constant K_e can be obtained, with concentration c, by the equation (6) below:

$$DP_N = \frac{1}{\sqrt{1-\alpha(T)}} = \frac{1}{2} + \frac{1}{2}\sqrt{4K_e(T)c + 1} \quad (6)$$

S3. Experimental Section

A. Materials and Reagents

1-Bromohexadecane, methyl gallate, methyllithium, tosyl chloride, triethylene glycol monomethyl ether, 5-bromo-1,2,3-trimethoxybenzene, boron tribromide, 2-acetyl-5-bromothiophene, bis(pinacolato)diboron, 5-bromo-2-thiophenecarboxylic acid, boron trifluoride-diethyl ether solution and potassium *tert*-butoxide (*t*-BuOK) were purchased from Energy Chemical Co, Ltd. Potassium carbonate (K_2CO_3), sodium hydroxide (NaOH), and sodium sulphate (Na_2SO_4) were the products of Beijing Chemical Reagent Company.

The precursors were prepared according to the modified literatures. [5–9]

B. Synthesis

The diketone ligands **L1**–**L4** were synthesized via related ketones and esters via Claisen condensation reaction according to previous literature reports.[5–9] The arylthiophenes were synthesized by the initial preparation of boronic acid ester-substituted derivatives followed by Suzuki cross-coupling reaction.[7] The synthetic routes for **L1**–**L4** are shown in Scheme S1.

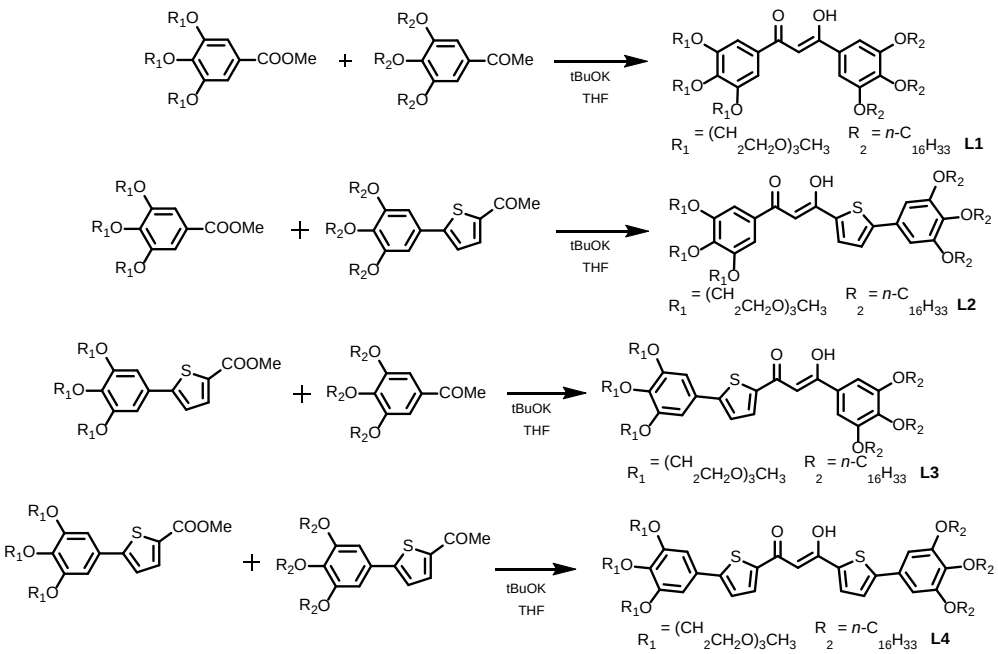

Scheme S1. Synthetic route for **L1**–**L4**.

C. Experimental Procedures

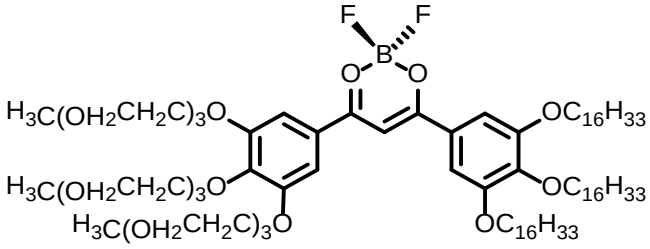

1. To a degassed anhydrous dichloromethane (50 mL) solution of **L1** (540 mg, 0.28 mmol) was added $BF_3{\cdot}OEt_2$, and the resulting mixture was stirred overnight at room temperature. The reaction was quenched by the addition of water and was extracted with chloroform and washed with brine, and dried over anhydrous magnesium sulfate. After filtration and removal of the solvent, the crude product was purified by column chromatography on silica gel (100–200 mesh; dichloromethane–petroleum ether, 1:2 v/v). Further purification was achieved by recrystallization by layering methanol onto a concentrated dichloromethane solution to give the product as a green solid. Yield: 210 mg (38 %).

^{1}H NMR (400 MHz, $CDCl_3$, 298 K): δ / ppm = 0.88 (t, J = 6.7 Hz, 9H, $-CH_3$), 1.26 (m, 72H, $-CH_2-$), 1.49 (m, 7.7 Hz, 6H, $-CH_2-$), 1.80 (m, 6H, $-CH_2-$), 3.35 (s, 6H, $-OCH_3$), 3.37 (s, 3H, $-OCH_3$), 3.53 (m, 6H, $-OCH_2CH_2O-$), 3.68 (m, 18H, $-OCH_2CH_2O-$), 3.81 (t, J = 4.8 Hz, 2H, $-OCH_2CH_2O-$), 3.89 (t, J = 4.7 Hz, 4H, $-OCH_2CH_2O-$), 4.07 (t, J = 6.4 Hz, 4H, $-OCH_2$), 4.11 (t, J = 6.6 Hz, 4H, $-OCH_2$), 4.24 (t, J = 4.7 Hz, 4H, $-OCH_2CH_2O-$), 4.34 (t, J = 4.8 Hz, 2H, $-OCH_2CH_2O-$), 6.94 (s, 1H, diketone), 7.33 (s, 2H, phenyl), 7.41 (s, 2H, phenyl).

^{13}C{^{1}H} NMR (126 MHz, $CDCl_3$, 298 K): δ / ppm = 14.12, 22.70, 26.08, 29.03, 29.72, 30.07, 31.94, 59.0, 69.70, 70.14, 71.31, 71.94, 72.73, 73.88, 76.78, 77.16, 77.39, 107.99, 109.64, 152.73, 153.29.

^{11}B{^{1}H} NMR (160 $CDCl_3$, 298 K): δ / ppm = 1.23.

Positive-ion HR-ESI MS: calcd for $C_{84}H_{149}BF_2O_{17}$ *m/z* = 1479.0856; found 1479.0643 $[M+H]^+$.

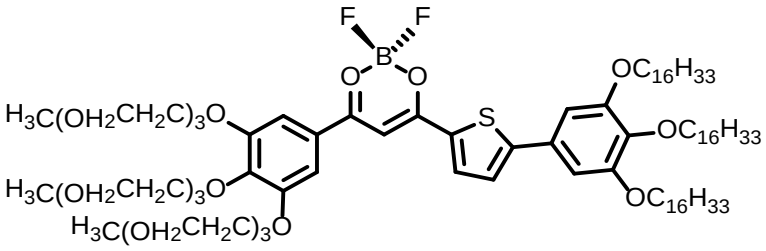

2. This was prepared according to a procedure similar to that described for **1**, expected **L2** (466 mg, 0.30 mmol) was used instead of **L1**. The product was isolated as an orange solid. Yield: 154 mg (32 %).

^{1}H NMR (500 MHz, $CDCl_3$, 298 K) : δ / ppm = 0.88 (t, J = 8.5 Hz, 9H, $-CH_3$), 1.26 (m, 72H, $-CH_2-$), 1.48 (m, 6H, $-CH_2-$), 1.79 (m, 6H, $-CH_2-$), 3.36 (s, 6H, $-OCH_3$), 3.37 (s, 3H, $-OCH_3$), 3.54 (m, 6H,

–OCH_2CH_2O–), 3.69 (m, 18H, –OCH_2CH_2O–), 3.81 (t, *J* = 6.0 Hz, 2H, –OCH_2CH_2O–), 3.89 (t, *J* = 6.0 Hz, 4H, –OCH_2CH_2O–), 4.01 (t, *J* = 8.0 Hz, 2H, –OCH_2), 4.04 (t, *J* = 8.2 Hz, 4H, –OCH_2), 4.27 (t, *J* = 6.0 Hz, 4H, –OCH_2CH_2O–), 4.33 (t, *J* = 6.0 Hz, 2H, –OCH_2CH_2O–), 6.87 (d, *J* = 5.0 Hz, 2H, phenyl), 7.38 (d, *J* = 5.2 Hz, 1H, thiophene), 7.39 (s, 2H, phenyl), 8.07 (d, *J* = 5.2 Hz, 1H, thiophene).

$^{13}C\{^1H\}$ NMR (126 MHz, $CDCl_3$, 298 K): δ / ppm = 14.13, 22.70, 26.13, 29.56, 30.36, 31.94, 59.02, 69.40, 69.71, 70.12, 71.17, 71.94, 76.78, 77.16, 105.30, 109.11, 153.71.

$^{11}B\{^1H\}$ NMR (160 $CDCl_3$, 298 K): δ / ppm = 1.01.

Positive-ion HR-ESI MS: calcd for $C_{88}H_{151}BF_2O_{17}S$ *m/z* = 1561.0733; found 1561.0425 $[M+H]^+$.

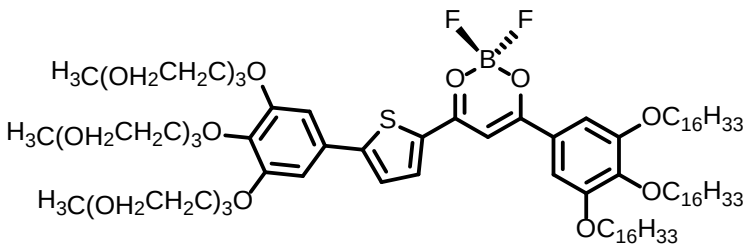

3. This was prepared according to a procedure similar to that described for **1**, expected **L3** (793 mg, 0.51 mmol) was used instead of **L1**. The product was isolated as an orange solid. Yield: 214 mg (27 %).

^1H NMR (400 MHz, $CDCl_3$, 298 K) : δ / ppm = 0.88 (t, *J* = 6.7 Hz, 9H, –CH_3), 1.26 (m, 72H, –CH_2–), 1.49 (m, 6H, –CH_2–), 1.80 (m, 6H, –CH_2–), 3.36 (s, 6H, –OCH_3), 3.37 (s, 3H, –OCH_3), 3.54 (m, 6H, –OCH_2CH_2O–), 3.70 (m, 18H, –OCH_2CH_2O–), 3.81 (t, *J* = 5.0 Hz, 2H, –OCH_2CH_2O–), 3.89 (t, *J* = 4.8 Hz, 4H, –OCH_2CH_2O–), 4.07 (t, *J* = 6.4 Hz, 4H, –OCH_2), 4.10 (t, *J* = 6.6 Hz, 2H, –OCH_2), 4.22 (t, *J* = 5.0 Hz, 2H, –OCH_2CH_2O–), 4.24 (t, *J* = 4.8 Hz, 4H, –OCH_2CH_2O–), 6.82 (s, 1H, diketone)), 6.95 (s, 2H, phenyl), 7.30 (s, 2H, phenyl), 7.36 (d, *J* = 4.2 Hz, 1H, thiophene), 8.20 (d, *J* = 4.2 Hz, 1H, thiophene).

$^{13}C\{^1H\}$ NMR (126 MHz, $CDCl_3$, 298 K): δ / ppm = 14.12, 22.70, 26.08, 28.98, 30.14, 30.40, 31.94, 59.03, 69.27, 69.72, 70.21, 71.26, 71.95, 72.56, 73.84, 76.80, 76.83, 77.70, 106.74, 107.60, 153.24.

$^{11}B\{^1H\}$ NMR (160 $CDCl_3$, 298 K): δ / ppm = 1.10.

Positive-ion HR-ESI MS: calcd for $C_{88}H_{151}BF_2O_{17}S$ *m/z* = 1561.0733; found 1561.0389 $[M+H]^+$

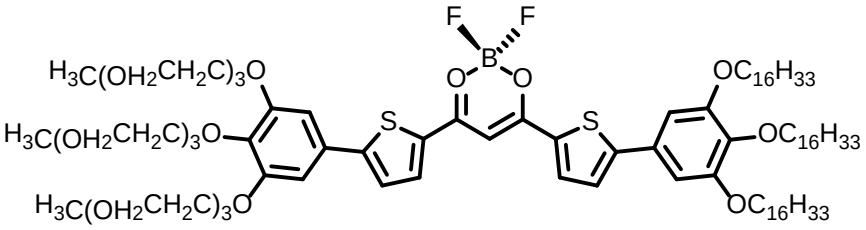

4. This was prepared according to a procedure similar to that described for **1**, expected **L4** (549 mg, 0.34 mmol) was used instead of **L1**. The product was isolated as an orange solid. Yield: 232 mg (41 %).

^{1}H NMR (400 MHz, $CDCl_3$, 298 K) : δ / ppm = 0.88 (t, J = 6.6 Hz, 9H, –CH_3), 1.26 (m, 72H, –CH_2–), 1.50 (m, 6H, –CH_2–), 1.81 (m, 6H, –CH_2–), 3.37 (s, 9H, –OCH_3), 3.55 (m, 6H, –OCH_2CH_2O–), 3.70 (m, 18H, –OCH_2CH_2O–), 3.82 (t, J = 5.0 Hz, 2H, –OCH_2CH_2O–), 3.89 (t, J = 4.8 Hz, 4H, –OCH_2CH_2O–), 4.01 (t, J = 6.6 Hz, 2H, –OCH_2), 4.04 (t, J = 6.4 Hz, 4H, –OCH_2), 4.22 (t, J = 5.0 Hz, 2H, –OCH_2CH_2O–), 4.24 (t, J = 4.8 Hz, 4H, –OCH_2CH_2O–), 6.73 (s, 1H, diketone)), 6.86 (s, 2H, phenyl), 6.94 (s, 2H, phenyl), 7.36 (d, J = 4.0 Hz, 2H, thiophene), 7.99 (m, 2H, thiophene).

^{13}C{^{1}H} NMR (126 MHz, $CDCl_3$, 298 K): δ / ppm = 14.13, 22.70, 26.12, 29.02, 30.15, 30.37, 31.94, 59.04, 69.22, 69.59, 70.64, 70.87, 71.95, 72.49, 76.78, 76.88, 77.16, 92.05, 101.01, 102.64, 105.93, 124.92, 135.38, 140.45, 153.22, 153.69.

^{11}B{^{1}H} NMR (160 $CDCl_3$, 298 K): δ / ppm = 0.84.

Positive-ion HR-ESI MS: calcd for $C_{92}H_{153}BF_2O_{17}S_2$ m/z = 1644.0644; found 1644.0328 $[M+H]^+$

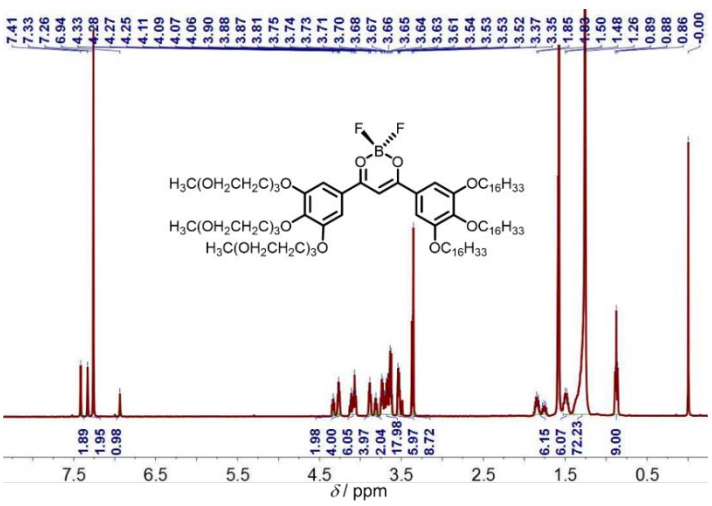

Figure S1. ^{1}H NMR spectrum of compound **1** in $CDCl_3$ at room temperature.

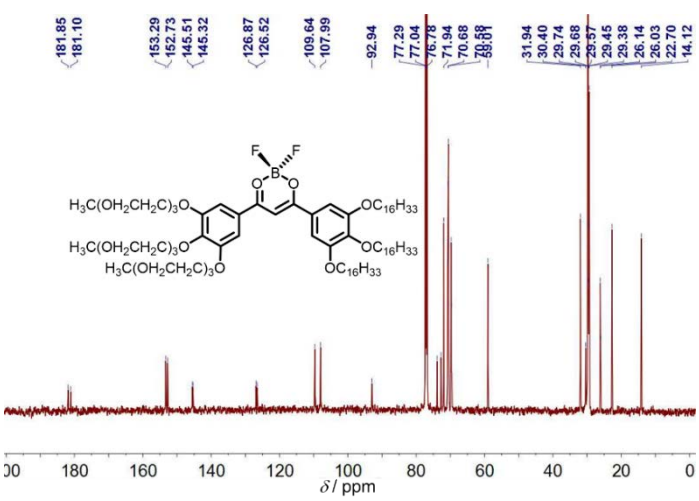

Figure S2. ^{13}C{^{1}H} NMR spectrum of compound **1** in $CDCl_3$ at room temperature.

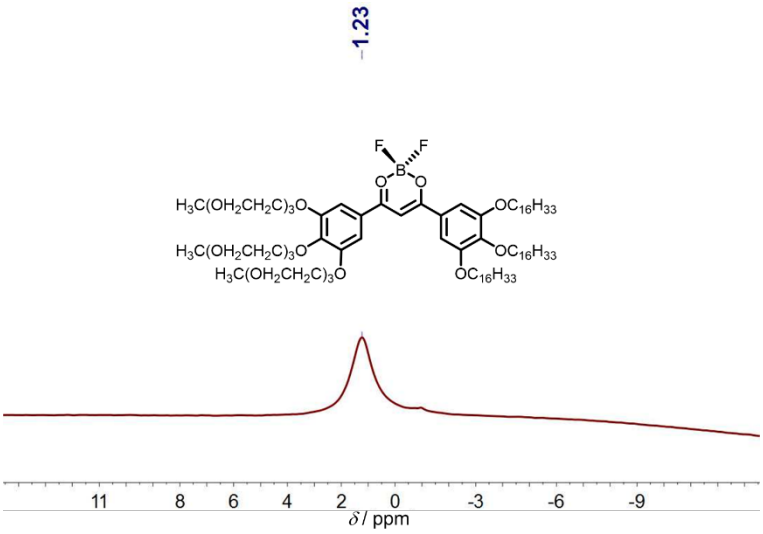

Figure S3. $^{11}B\{^{1}H\}$ NMR spectrum of compound **1** in $CDCl_3$ at room temperature.

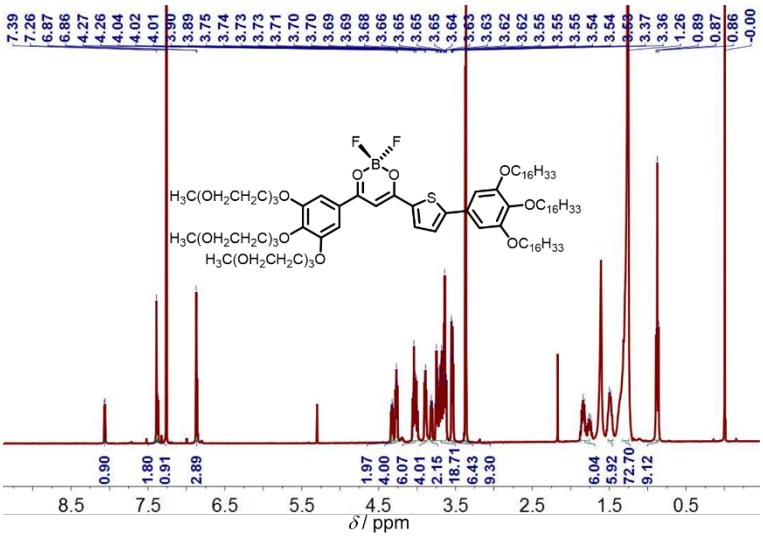

Figure S4. ^{1}H NMR spectrum of compound **2** in $CDCl_3$ at room temperature.

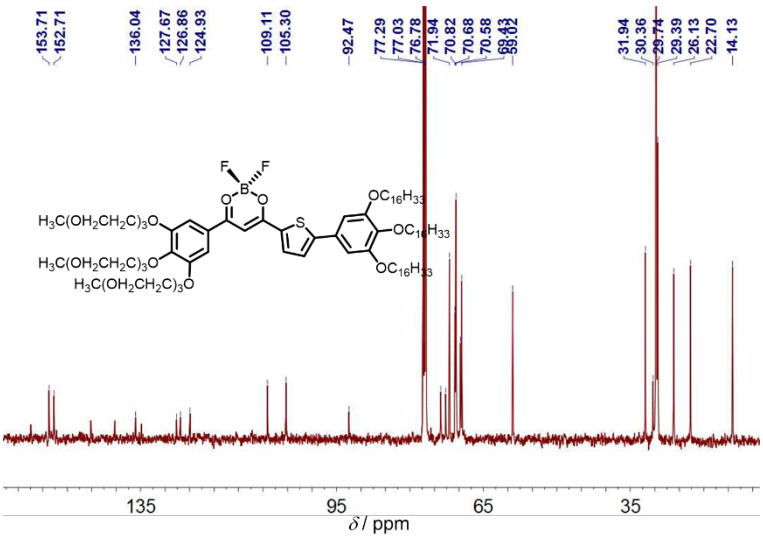

Figure S5. $^{13}C\{^{1}H\}$ NMR spectrum of compound **2** in $CDCl_3$ at room temperature.

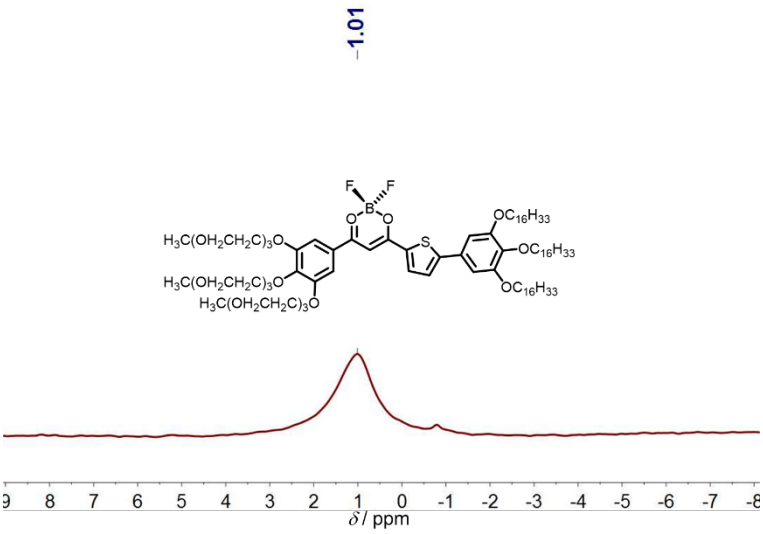

Figure S6. $^{11}B\{^1H\}$ NMR spectrum of compound **2** in $CDCl_3$ at room temperature.

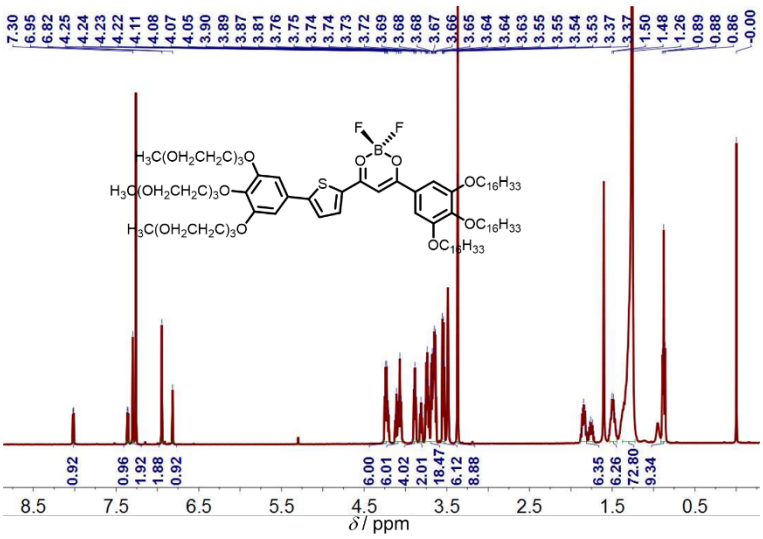

Figure S7. ^1H NMR spectrum of compound **3** in $CDCl_3$ at room temperature.

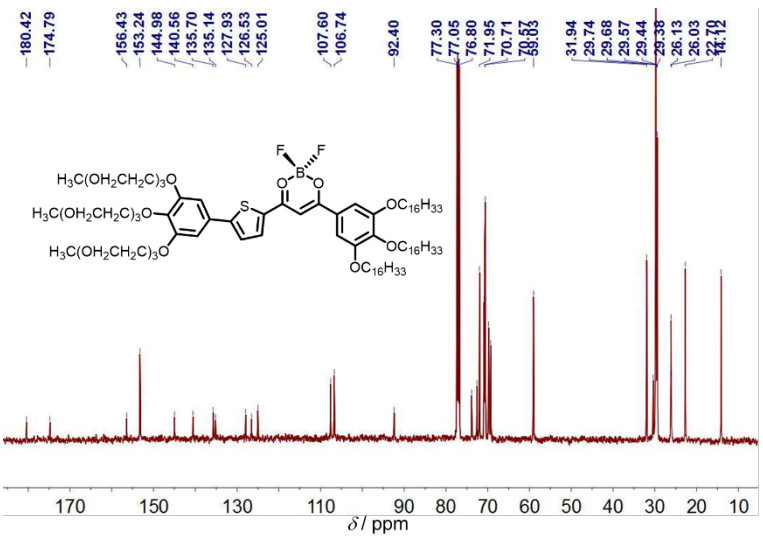

Figure S8. $^{13}C\{^1H\}$ NMR spectrum of compound **3** in $CDCl_3$ at room temperature.

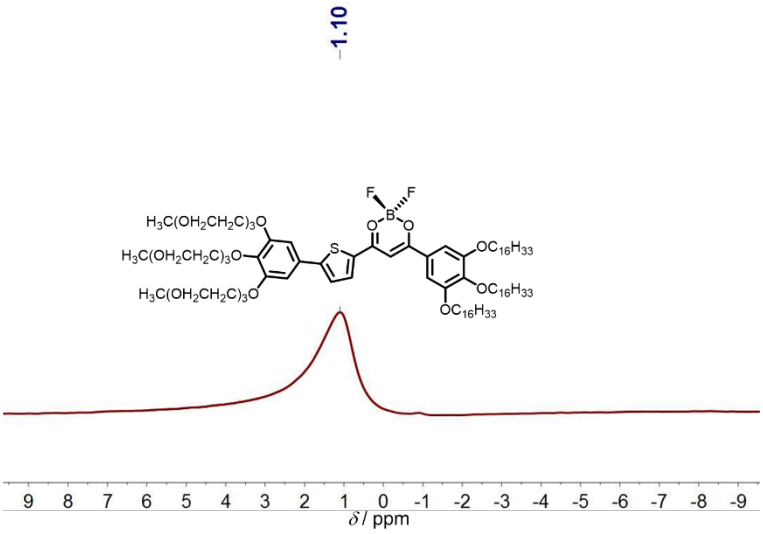

Figure S9. $^{11}B\{^{1}H\}$ NMR spectrum of compound **3** in $CDCl_3$ at room temperature.

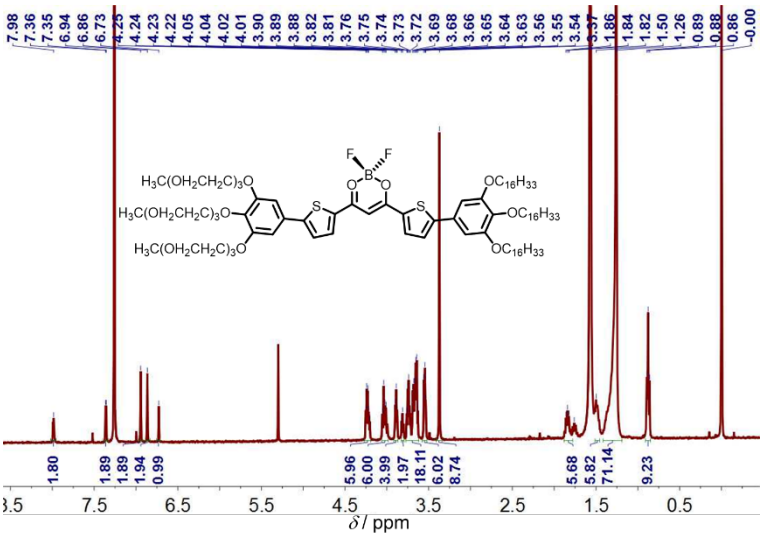

Figure S10. ^{1}H NMR spectrum of compound **4** in $CDCl_3$ at room temperature.

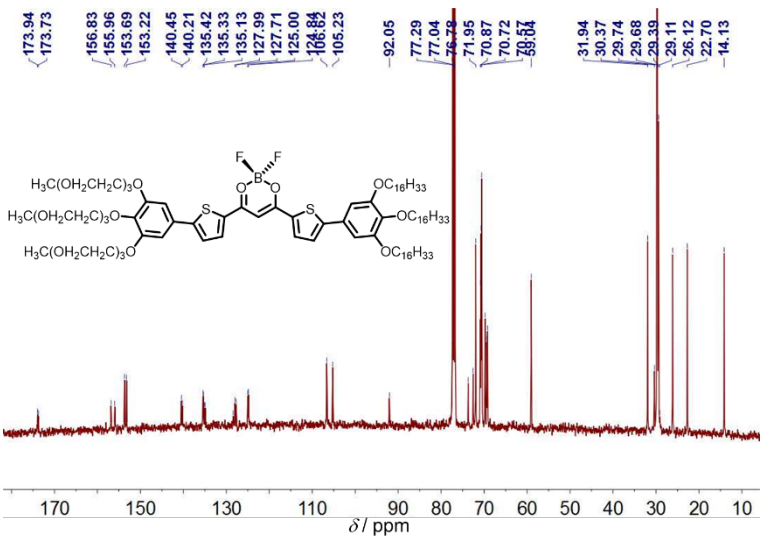

Figure S11. $^{13}C\{^{1}H\}$ NMR spectrum of compound **4** in $CDCl_3$ at room temperature.

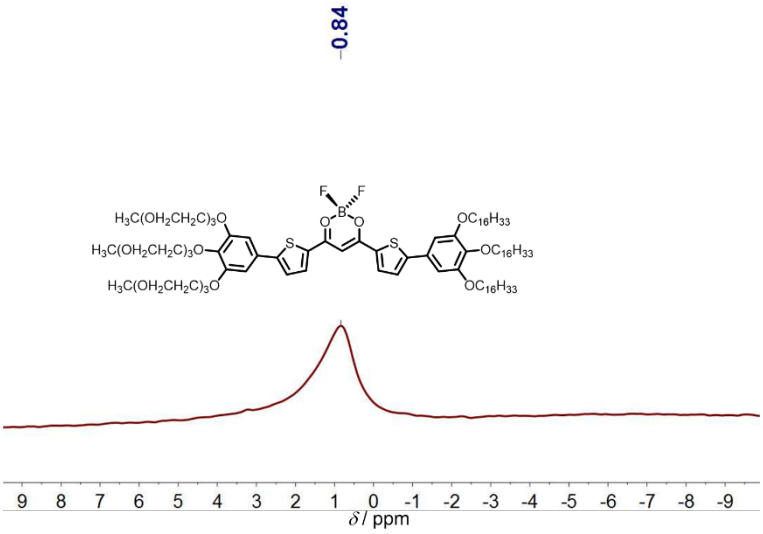

Figure S12. $^{11}B\{^{1}H\}$ NMR spectrum of compound **4** in $CDCl_3$ at room temperature.

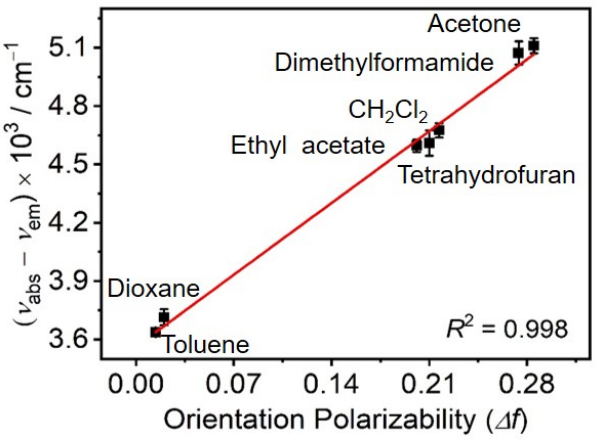

Figure S13. The Lippert–Mataga plot of compound **3**.

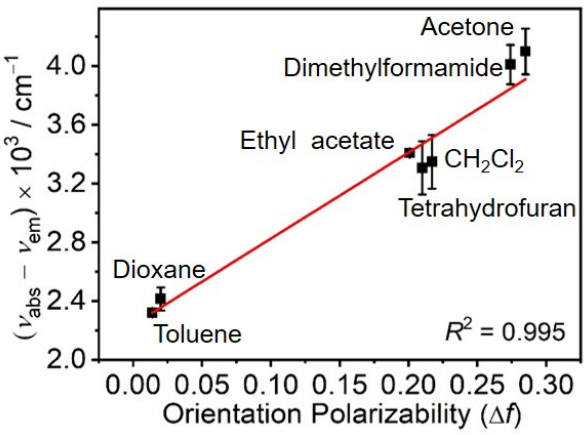

Figure S14. The Lippert–Mataga plot of compound **4**.

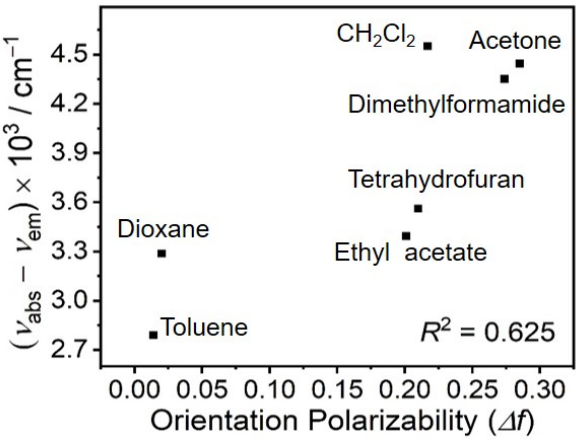

Figure S15. The Lippert–Mataga plot of compound **1**.

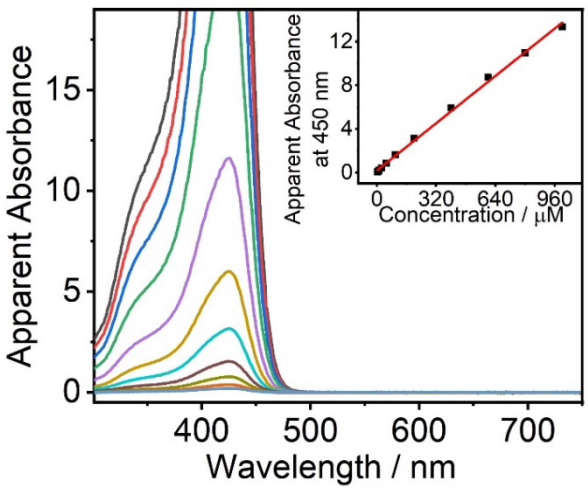

Figure S16. Electronic absorption spectra of **1** in THF solutions at the concentration range from 10^{-6} to 10^{-3} M. Inset: Plot of absorbance at 450 nm against concentration. The apparent absorbance values were obtained by correcting to 1-cm path length equivalence.

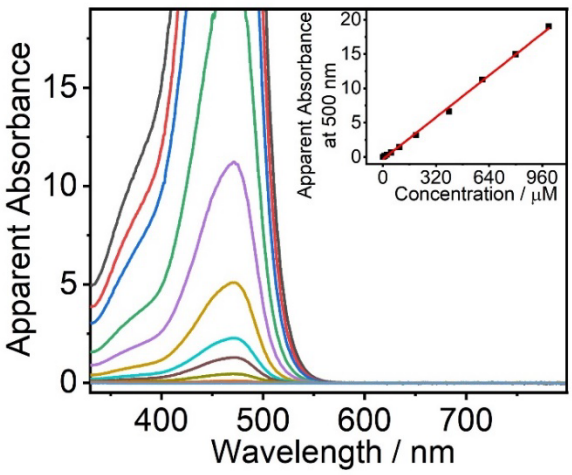

Figure S17. Electronic absorption spectra of **3** in THF solutions at the concentration range from 10^{-6} to 10^{-3} M. Inset: Plot of absorbance at 500 nm against concentration. The apparent absorbance values were obtained by correcting to 1-cm path length equivalence.

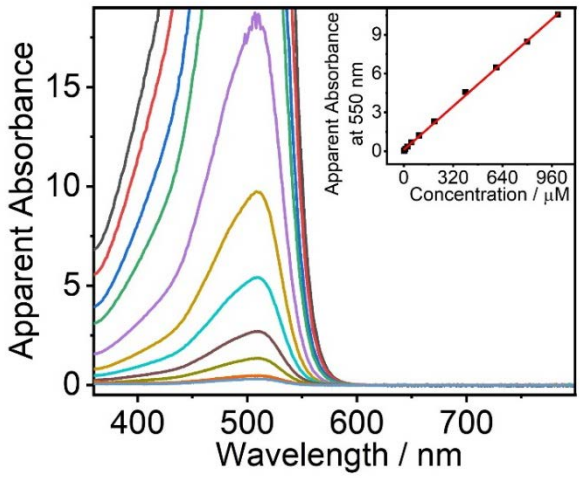

Figure S18. Electronic absorption spectra of **4** in THF solutions at the concentration range from 10^{-6} to 10^{-3} M. Inset: Plot of absorbance at 550 nm against concentration. The apparent absorbance values were obtained by correcting to 1-cm path length equivalence.

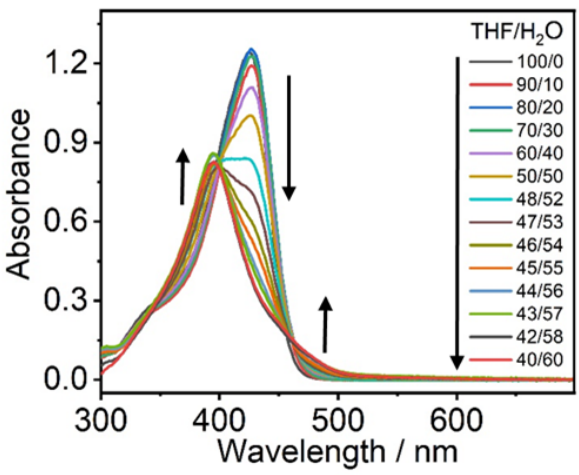

Figure S19. Electronic absorption spectra of **1** in THF solutions upon increasing water content from 0 (THF:H_2O, 100:0, v/v) to 60 % (THF:H_2O, 40:60, v/v) in the concentration range of 10^{-5} M.

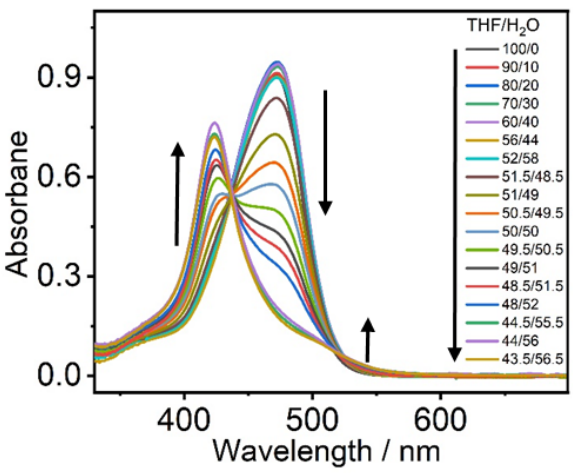

Figure S20. Electronic absorption spectra of **3** in THF solutions upon increasing water content from 0 (THF:H_2O, 100:0, v/v) to 56.5 % (THF:H_2O, 43.5:56.5, v/v) in the concentration range of 10^{-5} M.

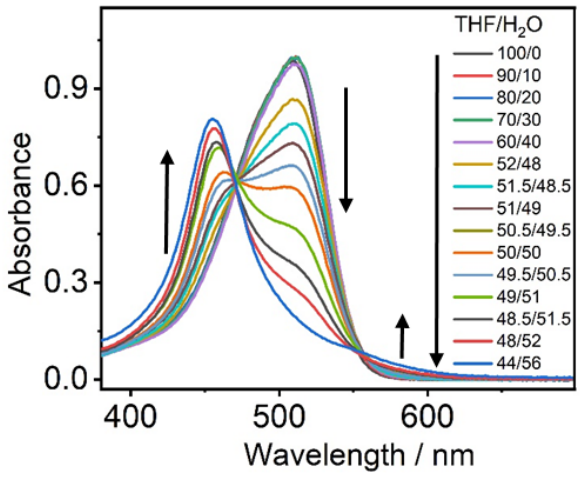

Figure S21. Electronic absorption spectra of **4** in THF solutions upon increasing water content from 0 (THF:H_2O, 100:0, v/v) to 56 % (THF:H_2O, 44:56, v/v) in the concentration range of 10^{-5} M.

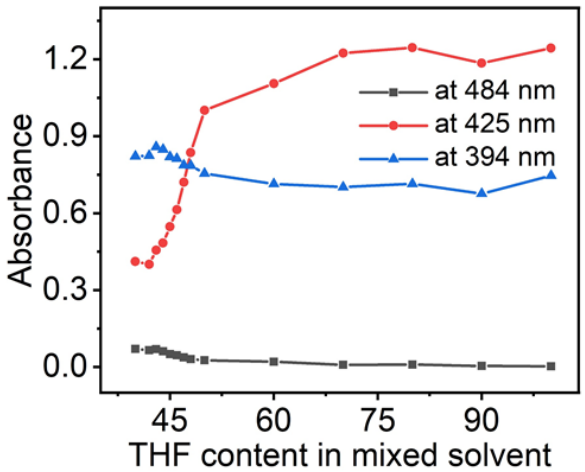

Figure S22. Electronic absorbance of **1** in THF solutions upon increasing water content from 0 (THF:H_2O, 100:0, v/v) to 56 % (THF:H_2O, 44:56, v/v) in the concentration range of 10^{-5} M at 484, 425 and 394 nm.

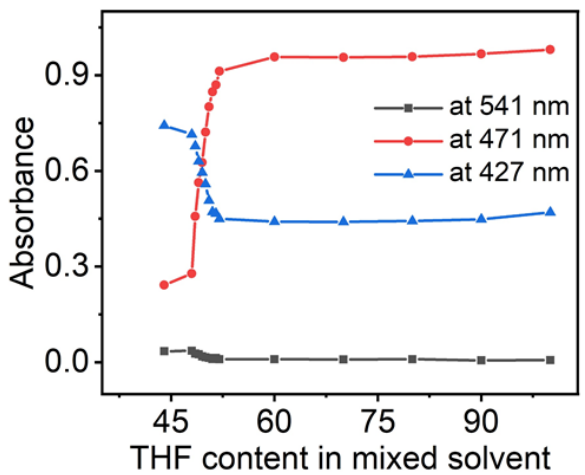

Figure S23. Electronic absorbance of **2** in THF solutions upon increasing water content from 0 (THF:H_2O, 100:0, v/v) to 56 % (THF:H_2O, 44:56, v/v) in the concentration range of 10^{-5} M at 541, 471 and 427 nm.

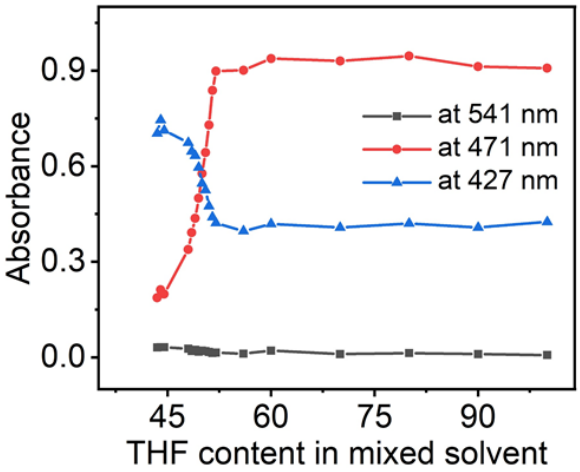

Figure S24. Electronic absorbance of **3** in THF solutions upon increasing water content from 0 (THF:H_2O, 100:0, v/v) to 56 % (THF:H_2O, 44:56, v/v) in the concentration range of 10^{-5} M at 541, 471 and 427 nm.

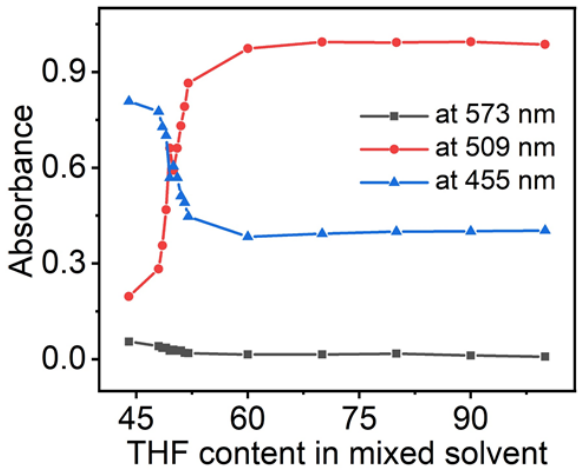

Figure S25. Electronic absorbance of **4** in THF solutions upon increasing water content from 0 (THF:H_2O, 100:0, v/v) to 56 % (THF:H_2O, 44:56, v/v) in the concentration range of 10^{-5} M at 573, 509 and 455 nm.

Figure S26. Photos showing the Tyndall effects of **1** in THF solutions upon increasing water content from 0 (THF:H_2O, 100:0, v/v) to 60 % (THF:H_2O, 40:60, v/v) in the concentration range of 10^{-5} M. (Number 1: 100% THF, 2: 90% THF, 3: 80% THF, 4: 70% THF, 5: 60% THF, 6: 50% THF, 7: 48% THF, 8: 47% THF, 9: 46% THF, 10: 45% THF, 11: 44% THF, 12: 43% THF, 13: 42% THF, 14: 40% THF.)

Figure S27. Photos showing the Tyndall effects of **2** in THF solutions upon increasing water content from 0 (THF:H_2O, 100:0, v/v) to 56 % (THF:H_2O, 44:56, v/v) in the concentration range of 10^{-5} M. (Number 1: 100% THF, 2: 90% THF, 3: 80% THF, 4: 70% THF, 5: 60% THF, 6: 52% THF, 7: 51.5% THF, 8: 51% THF, 9: 50.5% THF, 10: 50% THF, 11: 49.5% THF, 12: 49% THF, 13: 48.8% THF, 14: 48% THF, 15: 44% THF.)

Figure S28. Photos showing the Tyndall effects of **3** in THF solutions upon increasing water content from 0 (THF:H_2O, 100:0, v/v) to 56.5 % (THF:H_2O, 43.5:56.5, v/v) in the concentration range of 10^{-5} M. (Number 1: 100% THF, 2: 90% THF, 3: 80% THF, 4: 70% THF, 5: 60% THF, 6: 52% THF, 7: 51.5% THF, 8: 51% THF, 9: 50.5% THF, 10: 50% THF, 11: 49.5% THF, 12: 49% THF, 13: 48.8% THF, 14: 48% THF, 15: 44.5% THF, 16: 44% THF, 17: 43.5% THF.)

Figure S29. Photos showing the Tyndall effects of **4** in THF solutions upon increasing water content from 0 (THF:H_2O, 100:0, v/v) to 56 % (THF:H_2O, 44:56, v/v) in the concentration range of 10^{-5} M. (Number 1: 100% THF, 2: 90% THF, 3: 80% THF, 4: 70% THF, 5: 60% THF, 6: 52% THF, 7: 51.5% THF, 8: 51% THF, 9: 50.5% THF, 10: 50% THF, 11: 49.5% THF, 12: 49% THF, 13: 48.8% THF, 14: 48% THF, 15: 44% THF.)

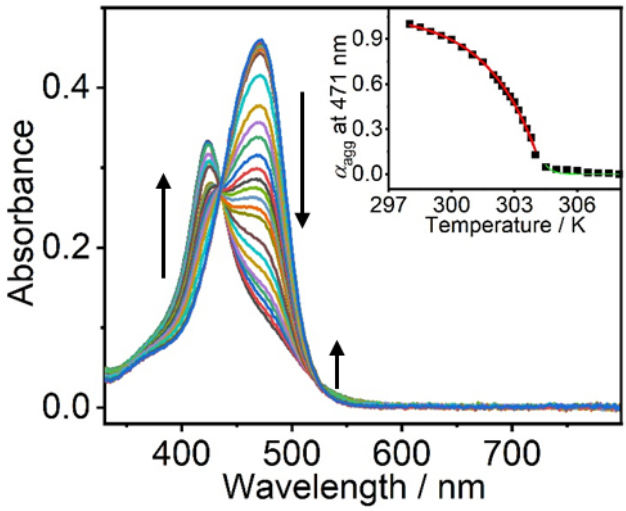

Figure S30. UV–Vis absorption spectral traces on cooling a solution of **3** in 44 % THF–water mixture (THF:H_2O, 44:56, v/v, 1.7×10^{-5} M) at a cooling rate of 0.25 K min^{-1}. (Inset) A plot of degree of aggregation at 471 nm as a function of temperature with the curve fitted at the elongation (red line) and nucleation (green line) regime based on the nucleation–elongation model.

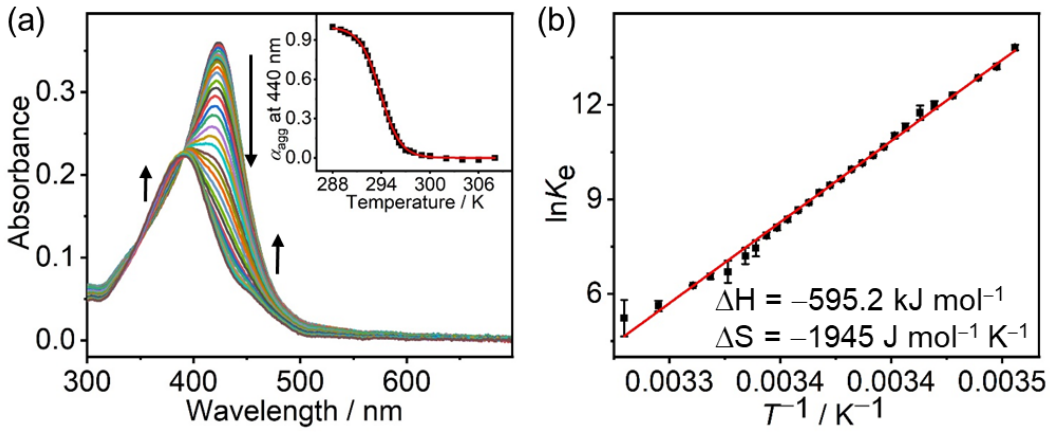

Figure S31. (a) UV–Vis absorption spectral traces on cooling a solution of **1** in 40 % THF–water mixture (THF:H_2O, 40:60, v/v, 3.9×10^{-5} M) at a cooling rate of 0.25 K min^{-1}. (Inset) A plot of degree of aggregation at 440 nm as a function of temperature with the curve fitted (red line) based on the temperature-dependent isodesmic model. (b) Van't Hoff plot of the equilibrium constant K_e at various temperatures with the corresponding thermodynamic parameters.

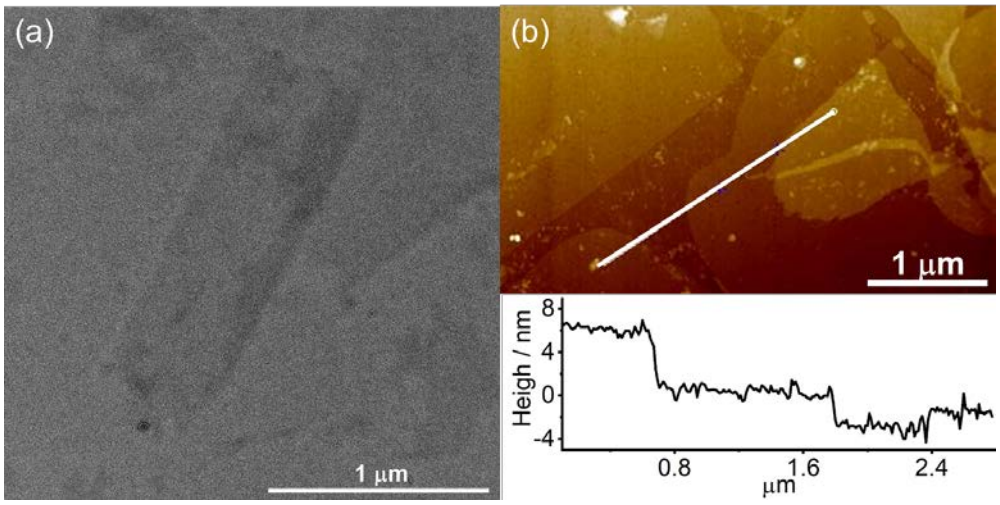

Figure S32. a) TEM image, b) AFM image and the corresponding height profile of compound **1** in 40 % THF–water mixture (THF:H_2O, 40:60, v/v).

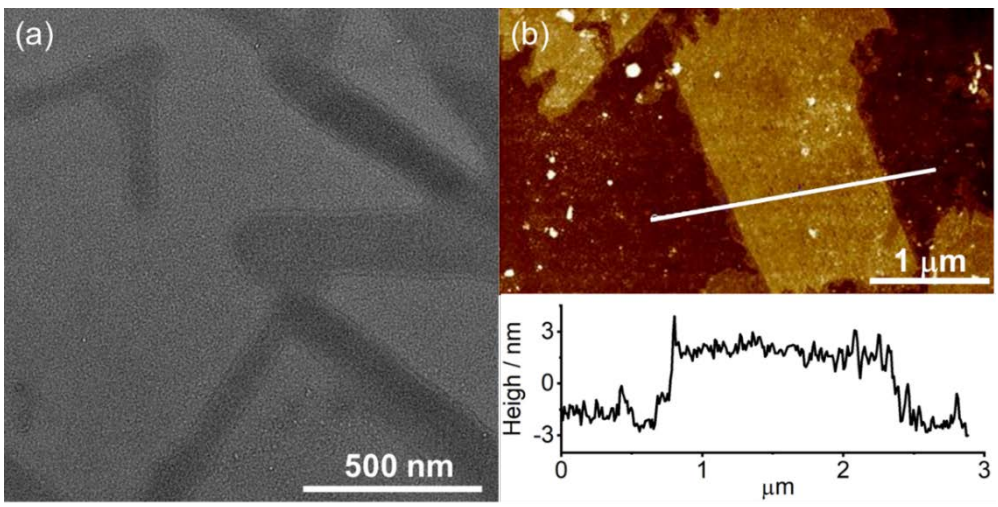

Figure S33. a) TEM image, b) AFM image and the corresponding height profile of compound **3** in 44 % THF–water mixture (THF:H_2O, 44:56, v/v).

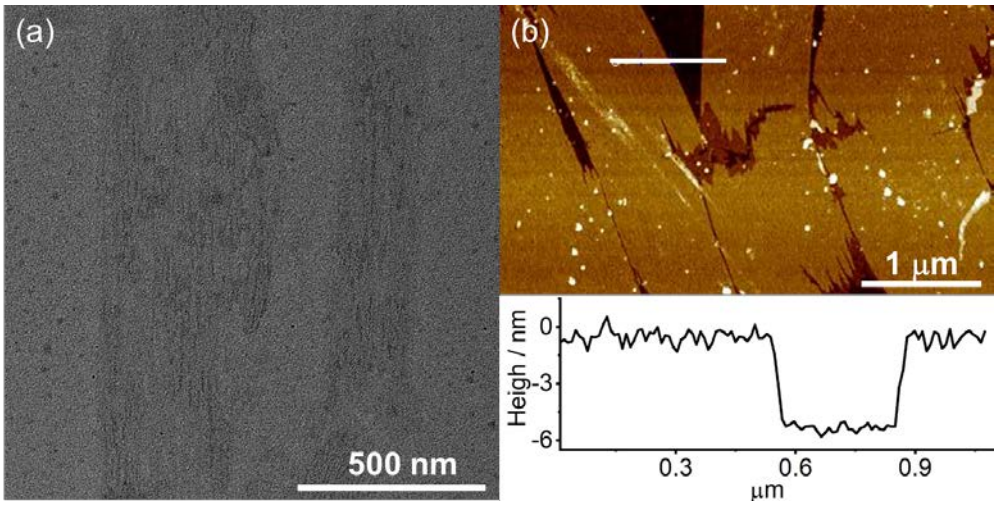

Figure S34. a) TEM image, b) AFM image and the corresponding height profile of compound **4** in 44 % THF–water mixture (THF:H_2O, 44:56, v/v).

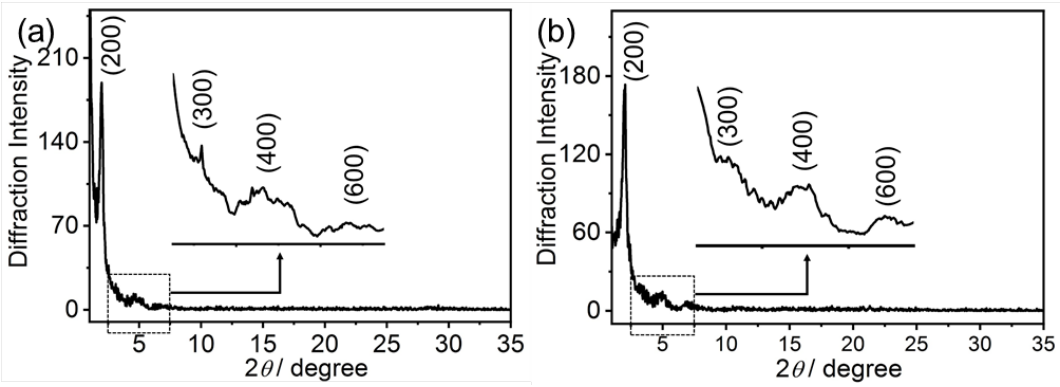

Figure S35. a) PXRD pattern of a thin film of compound **1** on a silicon wafer prepared by drop-casting, b) GI−XRD pattern of a thin film of compound **1** on a silicon wafer prepared by drop-casting.

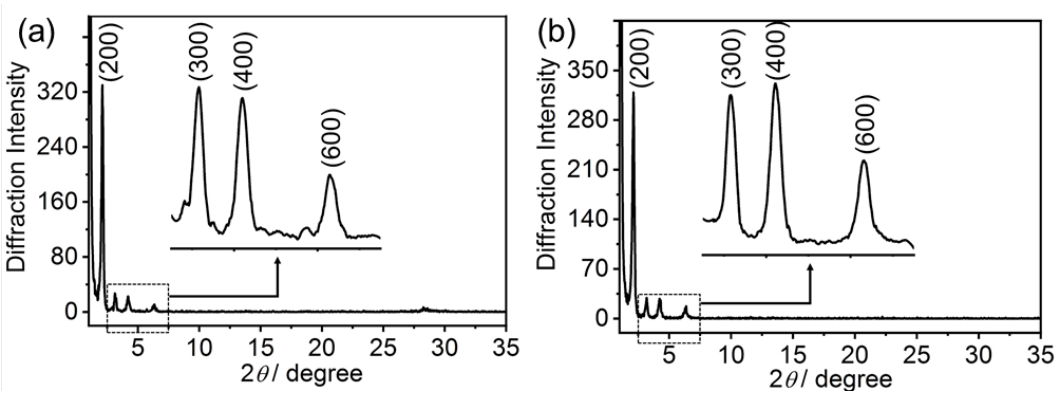

Figure S36. a) PXRD pattern of a thin film of compound **3** on a silicon wafer prepared by drop-casting, b) GI-XRD pattern of a thin film of compound **3** on a silicon wafer prepared by drop-casting.

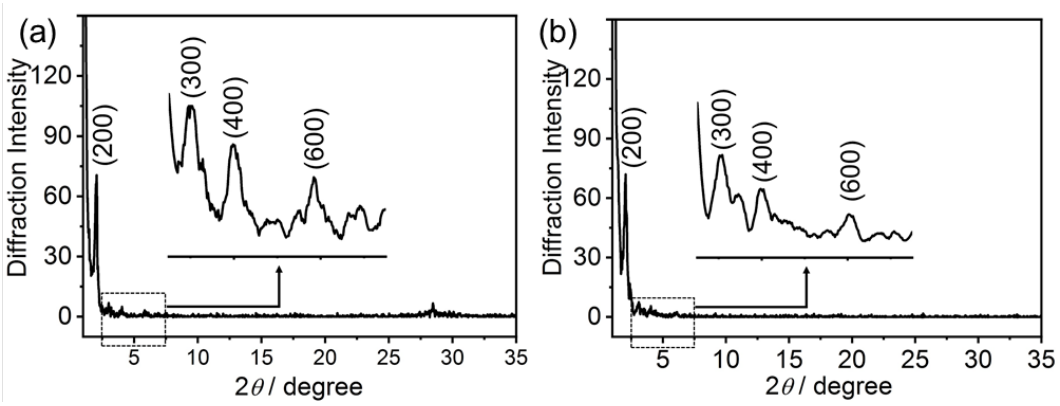

Figure S37. a) PXRD pattern of a thin film of compound **4** on a silicon wafer prepared by drop-casting, b) GI-XRD pattern of a thin film of compound **4** on a silicon wafer prepared by drop-casting.

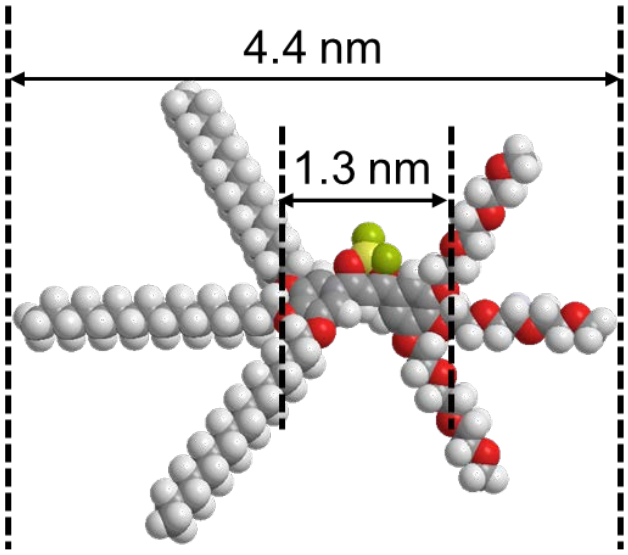

Figure S38. Computer-generated molecular model of **1**. Atom color code: white, H; grey, C; red, O; yellow, B; green, F.

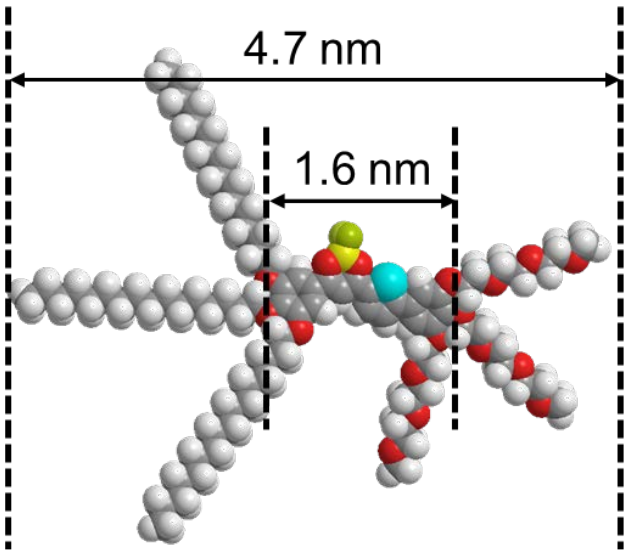

Figure S39. Computer-generated molecular model of **2**. Atom color code: white, H; grey, C; red, O; yellow, B; green, F; blue, S.

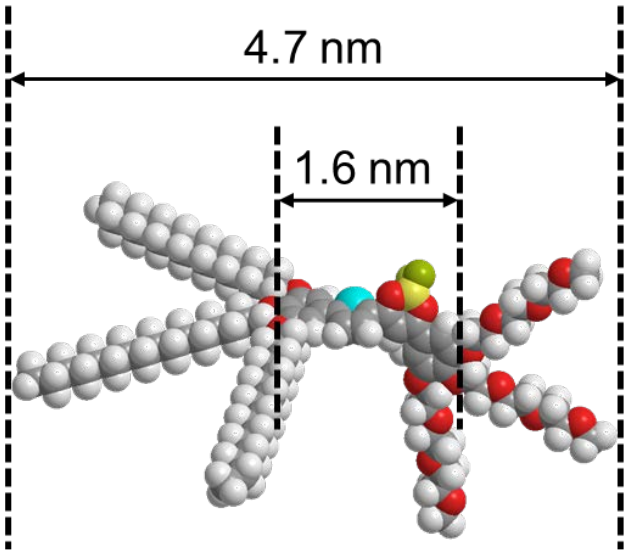

Figure S40. Computer-generated molecular model of **3**. Atom color code: white, H; grey, C; red, O; yellow, B; green, F; blue, S.

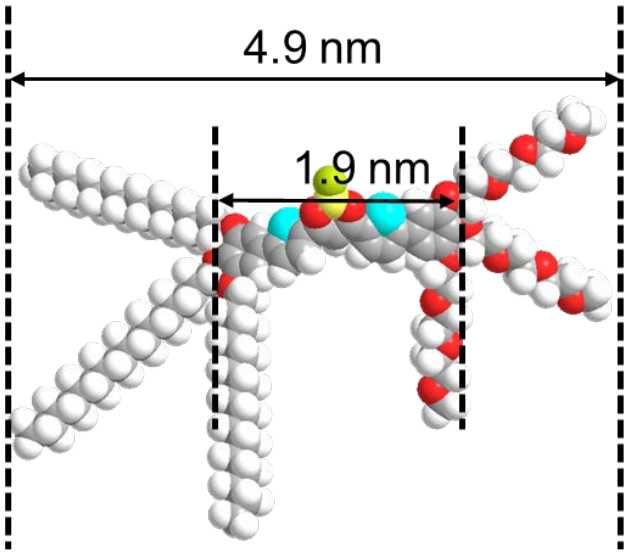

Figure S41. Computer-generated molecular model of **4**. Atom color code: white, H; grey, C; red, O; yellow, B; green, F; blue, S.

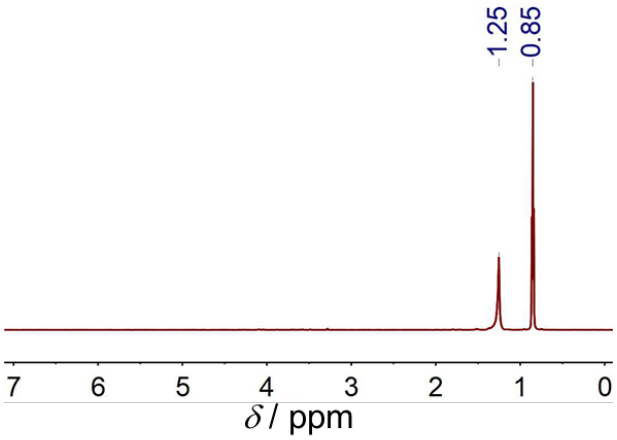

Figure S42. 1D NOE spectrum of **1** in D_2O–THF-d_8 (1:2, v/v) with irradiation at 0.85 ppm.

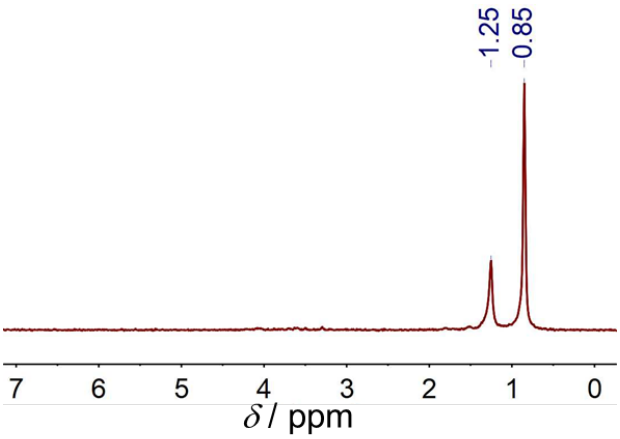

Figure S43. 1D NOE spectrum of **3** in D_2O–THF-d_8 (1:2, v/v) with irradiation at 0.85 ppm.

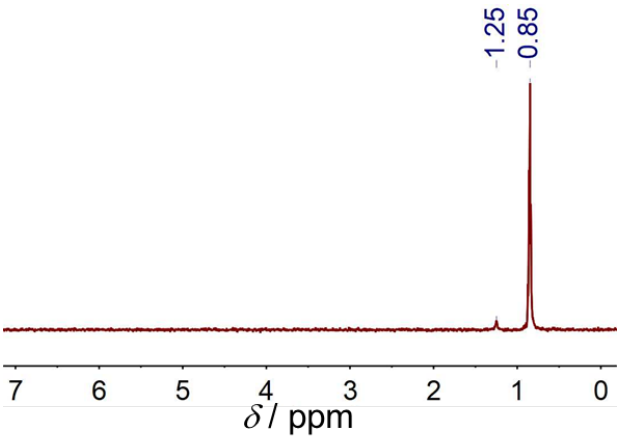

Figure S44. 1D NOE spectrum of **4** in D_2O–THF-d_8 (1:2, v/v) with irradiation at 0.85 ppm.

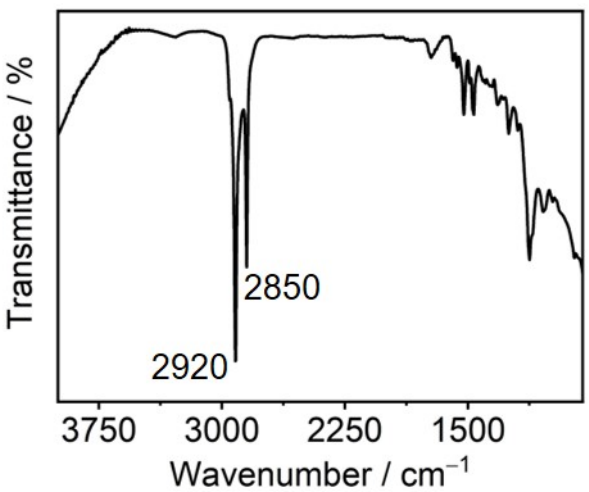

Figure S45. FTIR spectrum of a thin film of compound **1** on CaF_2 prepared by drop-casting.

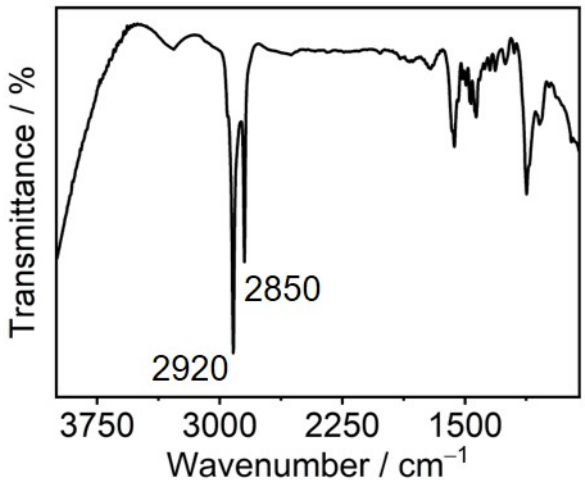

Figure S46. FTIR spectrum of a thin film of compound **3** on CaF_2 prepared by drop-casting.

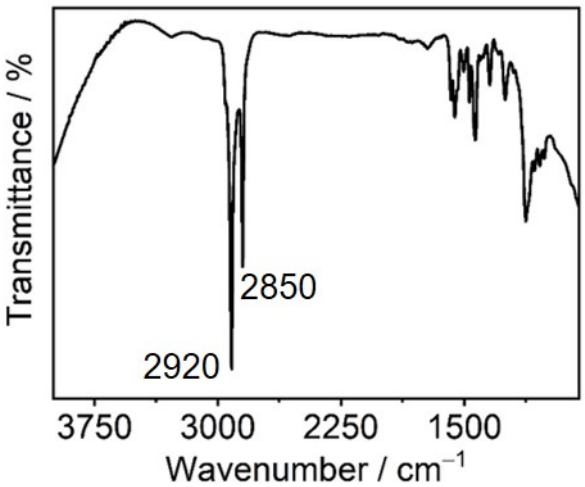

Figure S47. FTIR spectrum of a thin film of compound **4** on CaF_2 prepared by drop-casting.

Table S1. Photophysical data for **1**–**4** in different solvents at 298 K.

Compound	Medium	Absorption λ_{max} [nm][a]	Emission λ_{max} [nm]	Stokes Shift $\nu_{abs}-\nu_{em}$ [cm^{-1}]
1	Toluene	428	486	2800
	Dioxane	425	494	3300
	Ethyl acetate	426	498	3400
	Tetrahydrofuran	423	498	3600
	Dichloromethane	427	530	4600
	Dimethylfomamide	432	532	4400
	Acetone	427	527	4400
2	Toluene	470	561	3500
	Dioxane	471	566	3600
	Ethyl acetate	467	596	4600
	Tetrahydrofuran	471	598	4500
	Dichloromethane	472	603	4600
	Dimethylfomamide	485	645	5100
	Acetone	475	630	5200
3	Toluene	468	567	3600
	Dioxane	467	565	3700
	Ethyl acetate	466	593	4600
	Tetrahydrofuran	470	590	4600
	Dichloromethane	471	604	4700
	Dimethylfomamide	478	631	5000
	Acetone	472	622	5100
4	Toluene	505	572	2300
	Dioxane	508	579	2400
	Ethyl acetate	505	610	3400
	Tetrahydrofuran	509	612	3300

Dichloromethane	510	615	3300
Dimethylfomamide	520	657	4000
Acetone	512	648	4100

a. Refer to the lowest energy absorption band

Table S2. PXRD data for **1**–**4** on a silicon wafer prepared by drop-casting.

Compound	2θ (°)	d_{obs} (nm)	d_{cal} (nm)	*hkl*
1	2.18	4.05	4.05	(200)
	3.18	2.77	2.70	(300)
	4.34	2.03	2.03	(400)
	6.48	1.36	1.35	(600)
	28.60	0.312		
2	2.13	4.18	4.18	(200)
	3.16	2.79	2.79	(300)
	4.28	2.06	2.09	(400)
	6.32	1.40	1.39	(600)
	28.44	0.313		
3	2.10	4.20	4.20	(200)
	3.21	2.83	2.80	(300)
	4.20	2.10	2.10	(400)
	6.32	1.40	1.40	(600)
	28.24	0.316		
4	2.02	4.36	4.36	(200)
	3.09	2.87	2.90	(300)
	3.96	2.23	2.18	(400)
	5.98	1.48	1.45	(600)
	28.44	0.313		

Table S3. GI–XRD data for **1**–**4** on a silicon wafer prepared by drop-casting.

Compound	2θ (°)	d_{obs} (nm)	d_{cal} (nm)	*hkl*
1	2.18	4.05	4.05	(200)
	3.38	2.61	2.70	(300)
	4.68	1.89	2.03	(400)
	6.68	1.32	1.35	(600)
2	2.10	4.20	4.18	(200)
	3.14	2.81	2.79	(300)
	4.18	2.11	2.09	(400)
	6.28	1.41	1.39	(600)
3	2.12	4.16	4.20	(200)
	3.18	2.78	2.80	(300)
	4.22	2.09	2.10	(400)
	1.38	1.38	1.40	(600)
4	2.02	4.33	4.36	(200)
	3.06	2.88	2.90	(300)
	4.04	2.18	2.18	(400)
	6.10	1.45	1.45	(600)

References

1 J. N. Demas and G. A. Crosby, The measurement of photoluminescence quantum yields, *J. Phys. Chem.*, 1971, **75**, 991−1024.

2 J. V. Houten and R. J. Watts, Temperature dependence of the photophysical and photochemical properties of the tris(2,2'-bipyridy)ruthenium(II) ion in aqueous solution, *J. Am. Chem. Soc.*, 1976, **98**, 4853−4858.

3 P. Jonkheijm, P. van der Schoot, A. P. Schenning and E. W. Meijer, Probing the solvent-assisted nucleation pathway in chemical self-assembly, *Science*, 2006, **313**, 80−83.

4 M. M. Smulders, M. M. Nieuwenhuizen, T. F. de Greef, P. van der Schoot, A. P. Schenning and E. W. Meijer, How to distinguish isodesmic from cooperative supramolecular polymerisation, *Chem. Eur. J.*, 2010, **16**, 362−367.

5 D. S. Janni and M. K. Manheri, Hierarchical preferences of hydroxylated oxanorbornane-based achiral amphiphiles, *Langmuir*, 2013, **29**, 15182−15190.

6 X. J. Wang, L. B. Xing, F. Wang, G. X. Wang, B. Chen, C. H. Tung and L. Z. Wu, Multistimuli responsive micelles formed by a tetrathiafulvalene-functionalized amphiphile, *Langmuir*, 2011, **27**, 8665−8671.

7 T. Ishiyama, M. Murata and N. Miyaura, Palladium(0)-catalyzed cross-coupling reaction of alkoxydiboron with haloarenes: a direct procedure for arylboronic esters, *J. Org. Chem.*, 1995, **60**, 7508−7510.

8 H. Maeda, Y. Ito, Y. Haketa, N. Eifuku, E. Lee, M. Lee, T. Hashishin and K. Kaneko, Solvent-assisted organized structures based on amphiphilic anion-Responsive π-conjugated systems, *Chem. Eur. J*. 2009, **15**, 3706−3719.

9. I. Sánchez, J. A. Camp, J. V. Heras, M. Cano and E. Oliveira, Liquid crystal behavior induced in highly luminescent unsymmetrical borondifluoride β-diketonate materials, *Inorganica Chimica Acta*., 2012, **381**, 124−136.